Annexin A8 Regulates Late Endosome Organization and Function

Verena Goebeler,*†‡ Michaela Poeter,*† Dagmar Zeuschner,§∥ Volker Gerke,* and Ursula Rescher*

*Institute of Medical Biochemistry, Centre for Molecular Biology of Inflammation, and Interdisciplinary Clinical Research Centre, University of Muenster, 48149 Muenster, Germany; and §Department of Cell Biology, Institute of Biomembranes, University Medical Centre Utrecht, 3854 CX Utrecht, The Netherlands

Different classes of endosomes exhibit a characteristic intracellular steady-state distribution governed by interactions with the cytoskeleton. Late endosomes, organelles of the degradative lysosomal route, seem to require associated actin filaments for proper localization and function. We show here that the F-actin and phospholipid binding protein annexin A8 is associated specifically with late endosomes. Altering intracellular annexin A8 levels drastically affected the morphology and intracellular distribution of late endosomes. Trafficking through the degradative pathway was delayed in the absence of annexin A8, resulting in attenuated ligand-induced degradation of the epidermal growth factor receptor and prolonged epidermal growth factor-induced activation of mitogen-activated protein kinase. Depletion of annexin A8 reduced the association of late endosomal membranes with actin filaments. These results indicate that the defective cargo transport through the late endocytic pathway and the imbalanced signaling of activated receptors observed in the absence of annexin A8 results from the disturbed association of late endosomal membranes with the actin network, resulting in impaired actin-based late endosome motility.

INTRODUCTION

Surface receptors destined for degradation typically are removed from the plasma membrane after ligand binding and are routed toward the late endosomal/lysosomal system. For the epidermal growth factor (EGF) receptors (EGFRs), this process requires a specific sorting onto the membrane of internal vesicles of multivesicular endosomes that eventually fuse with lysosomal structures (Katzmann *et al.*, 2002). The sorting event also sequesters the EGFR-associated tyrosine kinase activity from the cytosol, thereby shutting off downstream signaling. Several components required for inward budding and sorting in multivesicular endosomes have been identified, mainly through the initial work on vacuolar protein sorting in yeast. They include the three endosomal sorting complexes required for sorting, ESCRT I to III, and the Vps27 protein Hrs in mammalian cells that recruits the sequentially acting ESCRT complexes to endosomal membranes (for reviews, see Gruenberg and Stenmark, 2004; van der Goot and Gruenberg, 2006; Piper and Katzmann, 2007; Piper and Luzio, 2007).

EGFR sorting requires the receptor-associated tyrosine kinase activity, and EGF has been shown to stimulate the biogenesis of a certain subpopulation of multivesicular endosomes that contain the sequestered EGFR (White *et al.*, 2006). This kinase-dependent sorting involves the cytosolic protein annexin A1, which serves as an EGFR substrate during this event (White *et al.*, 2006). Although annexin A1 thereby participates in the inward vesiculation process, a structurally related protein, annexin A2, has been implicated in the actual formation of multivesicular endosomes at the endosomal sorting compartment (Mayran *et al.*, 2003).

Annexins A1 and A2 are members of a multigene family of Ca^{2+}-regulated membrane binding proteins that participate in different membrane-related processes. All annexins share a conserved protein core that serves as a membrane docking module mediating the binding to membrane phospholipids with different annexins showing different phospholipid specificities. The second principal annexin domain is the N-terminal head region that is unique for each member and can serve as an interaction site for different protein ligands. This two domain structure enables annexins to recruit interacting proteins to certain membrane sites. Some annexins harbor binding sites for cytoskeletal proteins, and these members of the family have been implicated in membrane–cytoskeleton interactions (for reviews, see Hayes *et al.*, 2004; Rescher and Gerke, 2004; Gerke *et al.*, 2005). Annexin A8 is a so far poorly characterized annexin able to interact with phosphatidylinositides and F-actin in a Ca^{2+}-dependent manner, suggesting that it might function in coupling membranes to the actin cytoskeleton. In line with this property, it is specifically recruited to membrane sites that are associated with dynamic actin rearrangements in HeLa cells infected with enteropathogenic *Escherichia coli* (Goebeler *et al.*, 2006).

Here, we present evidence that annexin A8 is involved in the maintenance and physiological function of the late en-

dosomal/lysosomal compartment. Annexin A8 overexpression caused an increase in the average diameter and a clustering of late multivesicular endosomes in the perinuclear region, whereas depletion of endogenous annexin A8 resulted in a reduced average diameter of late endosomes and their relocation to the cell periphery. Importantly, annexin A8 depletion impaired EGF degradation and EGF-induced degradation of EGFR, resulting in sustained activation of extracellular signal-regulated kinase (ERK)1/2. Reduced copelleting of late endosomal membranes with F-actin in the annexin A8-depleted cells suggests that annexin A8 is involved in late endosome function by coupling endocytic membranes to the actin network.

MATERIALS AND METHODS

Mammalian Expression Constructs and Small Interfering RNAs (siRNAs)

The expression construct annexin A8-green fluorescent protein (GFP) (full-length human annexin A8 cDNA fused C terminally to GFP) has been described previously (Goebeler *et al.*, 2006). The annexin A8-specific siRNA duplex with 2-nt (2′-deoxy)-thymidine 3′ overhang corresponding to nucleotides 848–866 of the coding sequence of human annexin A8 was from Sigma –Aldrich (St. Louis, MO). Nontargeting control siRNA (siGenome nontargeting siRNA) and fluorescent control siRNA (siGLO) as a transfection indicator were obtained from Dharmacon RNA Technologies (Lafayette, CO).

Cell Culture, Transfection, and Drug Treatment

HeLa cells were maintained in DMEM with 10% fetal calf serum, 2 mM L-glutamine, 100 U/ml penicillin, and 100 μg/ml streptomycin in a 7% CO_2 incubator at 37°C. Cells were transfected with siRNA by using Oligofectamine (Invitrogen, Carlsbad, CA) according to the manufacturer's protocol and further cultivated for 48 h. Transfection frequency was routinely assessed by microscopic detection of cells transfected with fluorescent siGLO control siRNA (Dharmacon RNA Technologies) added to the siRNA transfection reactions and was typically >90%. For plasmid transfection, Effectene (QIAGEN, Valencia, CA) was used according to the manufacturer's protocol. For treatment with the actin-perturbing drugs latrunculin A (LTNA) and cytochalasin D (CD), cells were incubated for 10 min with 0.5 μM LTNA or for 15 min with 1 μM CD in culture medium at 37°C.

Labeling with Fluorescent Endocytosed Probes

HeLa cells expressing annexin A8-GFP for 24 h were incubated in internalization medium (minimal essential medium, 20 mM HEPES, pH 7.2, 0.8 mg/ml sodium bicarbonate, and 1 mg/ml bovine serum albumin [BSA]) containing 0.15 mg/ml DQ Red-BSA (Invitrogen) for 1 h and then chased overnight in culture medium. The bright fluorescence of this pH insensitive, strongly self-quenched dye is only seen after proteolytic cleavage in late endosomes. For visualizing EGF transport, cells were serum starved overnight and incubated with 2 μg/ml rhodamine-conjugated EGF (Invitrogen) for 10 min in serum-free culture medium, washed with phosphate-buffered saline (PBS), and either fixed immediately or chased for 4 h and then fixed. All incubations were carried out at 37°C.

Immunocytochemistry and Confocal Fluorescence Microscopy

Goat polyclonal anti-human annexin A8 antibody (c-20) was from Santa Cruz Biotechnology (Santa Cruz, CA). Anti-actin antibody clone AC-15 was from Sigma-Aldrich. The mouse monoclonal antibodies against human lysosome-associated membrane protein (LAMP) 1 and LAMP3/CD63, clones H4A3 and H5C6, respectively, were obtained from the Developmental Studies Hybridoma Bank (University of Iowa, Iowa City, IA). Mouse monoclonal antibody (mAb) against LBPA (Kobayashi *et al.*, 1998) was kindly provided by Jean Gruenberg (University of Geneva, Geneva, Switzerland). HeLa cells grown on coverslips were fixed with methanol (−20°C) for 2 min followed by an additional fixation step with 4% paraformaldehyde (PFA) in PBS for 10 min. Fixed cells were blocked with 2% BSA in PBS for 20 min and then incubated with primary antibodies at room temperature for 60 min. The cells were then washed with PBS and incubated at room temperature for 40 min with the appropriate secondary antibody coupled to Texas Red or Cy2. Confocal microscopy was performed using an LSM 510 META microscope (Carl Zeiss, Jena, Germany) equipped with a Plan-Apochromat 63×/1.4 oil immersion objective. For the size of LAMP1-positive endosomes, for each experimental condition, 10 cells were randomly chosen, and the diameter of 20 LAMP1-positive vesicles/cell was measured using the LSM3.2 software (Carl Zeiss). Giant vesicles were defined by a diameter size ≥1.6 μm. Statistical significance of the results was evaluated by unpaired Student's *t* tests. To quantify

the association of annexin A8-GFP with the endosomes and the plasma membrane, digital images were imported in MetaMorph (Molecular Devices, Sunnyvale, CA) and thresholded for each cell to define and exclude cytosolic background pixel intensity. For each cell, the outlines were defined, and all pixels of the annexin A8 signal with intensities above the threshold were recorded. Nuclear signals were subtracted to obtain the integrated gray value intensity of total cellular membrane-bound annexin A8-GFP. Next, the integrated gray value intensities of the plasma membrane regions were recorded and subtracted from the total membrane intensity, resulting in the endosomal gray value of annexin A8-GFP association. Signals of the different compartments were calculated as percentage of total membrane-bound annexin A8-GFP for a given cell. Data were collected from 20 cells out of >10 independent transfection experiments. The statistical significance of the results was evaluated by unpaired *t* tests.

Cryoimmunoelectron Microscopy

Cells were prefixed in 4% PFA and 0.4% glutaraldehyde (GA) in 0.1 M phosphate buffer, pH 7.4, for 10 min. Subsequently, cells were fixed using 2% PFA and 0.2% GA in 0.1 M phosphate buffer, pH 7.4, for 2 h at room temperature. Fixed cells were washed with PBS, and free aldehyde groups were quenched with 50 mM glycine in PBS. Cells were scraped in PBS containing 1% gelatin and pelleted in 12% gelatin. The cell pellets were solidified on ice and cut into small blocks, which were incubated for cryo-protection overnight at 4°C in 2.3 M sucrose. Blocks were mounted on aluminum pins and frozen in liquid nitrogen. Ultrathin cryosectioning and immunogold labeling were done as described using a polyclonal antibody against GFP from Invitrogen (Slot *et al.*, 1991; Liou *et al.*, 1996).

EGF Degradation Assay

Cells were serum starved overnight and incubated with 1 ng/ml ^{125}I-EGF (PerkinElmer Life and Analytical Sciences, Boston, MA) for 10 min at 37°C in serum-free medium, acid stripped at 4°C to remove surface-bound EGF (0.1 M glycine, pH 3.0, and 0.9% NaCl), and further chased for the indicated periods. Determination of ^{125}I-EGF degradation was carried out essentially as described previously (White *et al.*, 2006). Briefly, incubation media were collected and proteins were precipitated with 20% trichloroacetic acid (TCA). Cells were lysed with 1% Triton X-100 for 10 min at 4°C. ^{125}I-EGF degradation was determined as ratio of TCA-soluble counts in the medium (degradation products) to total counts in the lysates. Statistical significance of the results from four independent experiments was evaluated by unpaired Student's *t* tests.

Analysis of Annexin A8 RNA Interference (RNAi), EGFR Degradation, and ERK1/2 Activation

To analyze EGFR degradation, cells were serum starved overnight and incubated with 100 ng/ml EGF (BIOMOL Research Laboratories, Plymouth Meeting, PA) and 10 μg/ml cycloheximide for the indicated periods. Cells were then scraped in ice-cold PBS, pelleted, resuspended in 8 M urea, and sonicated. Equal amounts of total cellular protein were analyzed by SDS-polyacrylamide gel electrophoresis (PAGE) and subsequent immunoblotting using rabbit polyclonal anti-EGF receptor antibody (sc-03; Santa Cruz Biotechnology). To investigate activation of the mitogen-activated protein (MAP) kinases ERK1/2, the membranes were probed with rabbit anti-phospho-ERK1/2 antibodies and subsequently stripped and reprobed for total ERK (mouse monoclonal phospho-p42/44 and rabbit polyclonal p42/44; Cell Signaling Technology, Danvers, MA) as described previously (Lange *et al.*, 2007). Remaining EGFR levels after stimulation were analyzed by quantifying the intensities of the 180-kDa band representing the mature EGFR. Phospho-ERK1/2 levels were normalized to total ERK levels in the corresponding samples. RNAi efficiency was assessed with goat polyclonal anti-human annexin A8 antibody from Santa Cruz Biotechnology. Detection of vimentin using monoclonal anti-vimentin antibody (Dianova, Hamburg, Germany) was included as internal loading control. Signal intensities were quantified by densitometric analysis using the ImageJ software (National Institutes of Health, Bethesda, MD). Statistical significance of the results obtained from five independent experiments was evaluated by unpaired Student's *t* test.

Subcellular Fractionation

Cells expressing annexin A8-GFP were lysed in 10 mM Tris-HCL, pH 7.4, with added protease inhibitor cocktail (Roche Diagnostics, Mannheim, Germany) by passage through a 23-gauge needle. When indicated, Ca^{2+} was added to a final concentration of 500 μM. Postnuclear supernatants (PNS) were prepared by centrifugation of the lysates for 10 min at 1000 × *g*. Membranes were pelleted by centrifugation of PNS for 60 min at 100,000 × *g*. Equal protein amounts of PNS, the resuspended membrane pellets, and the final supernatants were analyzed by SDS-PAGE and subsequent immunoblotting using goat polyclonal anti-human annexin A8 antibody (c-20; Santa Cruz Biotechnology) and anti-LAMP2 antibody (clone H4B4; Developmental Studies Hybridoma Bank). Amounts of annexin A8-GFP in the different fractions were quantified by densitometric scanning using the ImageJ software (National Institutes of Health) and calculated as percentage of total annexin A8-GFP detected in the fractionation. Statistical significance of the
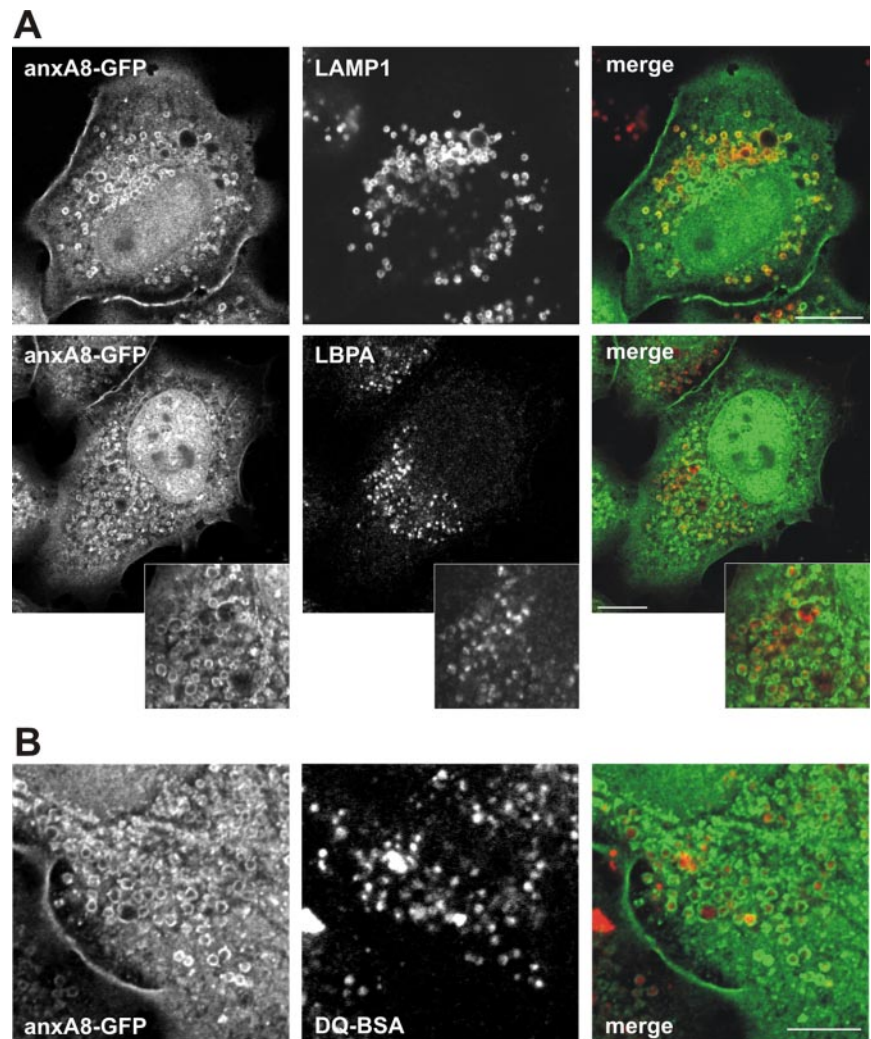
Figure 1. Annexin A8-GFP localizes to multivesicular late endosomes. (A) HeLa cells expressing annexin A8-GFP were stained with either anti-LAMP1 or anti-LBPA antibodies. Bars, 10 μm, insets show a 2.5-fold magnification. To visualize endosomes with proteolytic activity, cells shown in B were loaded for 1 h with DQ Red-BSA, washed, and incubated overnight in culture medium. The pH-insensitive dye coupled to BSA is strongly self-quenched and only fluoresces upon proteolytic cleavage and release of single peptides. Bar, 5 μm. All panels show single confocal sections.

results obtained from at least five independent experiments was evaluated by unpaired Student's *t* test.

Fractionation of Actin-associated Membranes

The actin-associated late endosomal membrane fraction was prepared essentially as described previously (Richardson *et al.*, 2004; Holtta-Vuori *et al.*, 2005). Briefly, postnuclear supernatants were prepared by lysing cells in 10 mM Tris-HCl, pH 7.4, 1 mM magnesium acetate, and protease inhibitor cocktail (Roche Diagnostics) by passage through a 23-gauge needle and centrifugation for 15 min at 600 $\times$ *g*. Nocodazole (100 μM) was added for 30 min at 37°C to depolymerize microtubules. Membranes were pelleted at 100,000 $\times$ *g* for 5 min. Amounts of actin, LAMP2, and tubulin in the postnuclear supernatants as well as in the membrane fractions were detected by immunoblotting using the respective antibodies (anti-actin, clone AC-15 [Sigma-Aldrich]; anti-LAMP2, clone H4B4 [Developmental Studies Hybridoma Bank]; anti-tubulin, clone YL1/2) and quantified by densitometric scanning using the ImageJ software (National Institutes of Health). To normalize the different experiments, LAMP2 and actin signals in the pelleted membranes were calculated as percentage of input. Bars represent the mean amount $\pm$ SEM of actin-associated LAMP2 in the pellets of 11 independent experiments. Statistical significance of the results was evaluated by unpaired Student's *t* test.

RESULTS

Annexin A8-GFP Localizes to Multivesicular Late Endosomes

To visualize the subcellular localization and identify the specific cellular target membranes of annexin A8, we expressed annexin A8 C terminally fused with GFP (Goebeler

et al., 2006) in HeLa cells. In these cells, low levels of endogenous annexin A8 are detectable (our unpublished data). Confocal laser scanning microscopy revealed that, in addition to some diffuse background signal of apparently non-membrane-associated protein, annexin A8-GFP localized to the plasma membrane and to large ring-shaped vesicular structures (Figure 1). These vesicles were distributed throughout the whole cell but seemed more concentrated in the perinuclear region, a pattern reminiscent of late endosomal compartments. Therefore, we used well-established markers for late endosomal organelles. Annexin A8-GFP–positive vesicles largely colocalized with LAMP1 and LAMP2, membrane glycoproteins that are two of the most abundant proteins found both in late endosomes and lysosomes (Griffiths *et al.*, 1988), and the late endosomal tetraspanin LAMP3 (Escola *et al.*, 1998) (Figure 1A; our unpublished data). Immunofluorescence staining of the endogenous annexin A8 protein revealed a similar colocalization (our unpublished data). Annexin A8-GFP also showed a high degree of colocalization with LBPA, a poorly degradable phospholipid found exclusively on the internal membranes of multivesicular late endosomes (Kobayashi *et al.*, 1998; Matsuo *et al.*, 2004), with the ring-shaped annexin A8-GFP signal surrounding LBPA-positive smaller sphere-shaped internal vesicles (Figure 1A). In contrast, we observed only a very
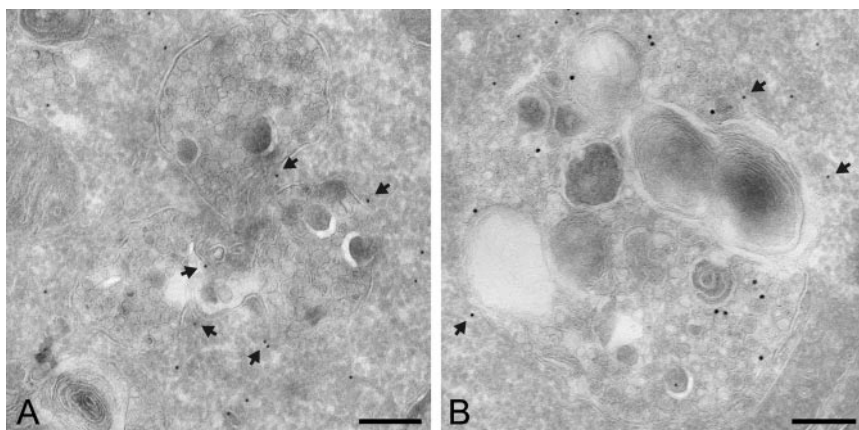
Figure 2. Annexin A8-GFP is found on the limiting membrane of late endosomes. Ultrathin cryosections of HeLa cells were immunogold labeled for annexin A8-GFP and LBPA. (A) Annexin A8-GFP can be found on the limiting membranes of late endosomes (arrows). (B) Annexin A8-GFP (10-nm protein A gold; arrows) localized to the limiting membranes of late endosomes that contained LBPA-enriched internal vesicles (15-nm protein A gold). Bars, 200 nm.

limited colabeling with early endosomal antigen 1, Rab11, or transferrin receptor, established markers of the early/recycling endosomal compartment (data not shown). Thus, in addition to the plasma membrane, annexin A8 seems to be specifically associated with the limiting membranes of multivesicular late endosomes. To confirm that the annexin A8-GFP–positive vesicles are accessible to cargo destined for degradation in the lysosomal pathway, we used DQ Red-BSA, a substrate that heavily self-quenches and requires enzymatic cleavage in an acidic intracellular compartment to generate a fluorescent product. As shown in Figure 1B, DQ Red-BSA was found in annexin A8-GFP-surrounded endosomes further supporting the conclusion that these vesicles were of late endosomal origin.

To analyze the endosomal annexin A8 localization in more detail, we performed double immunogold labeling on ultrathin cryosections of HeLa cells for electron microscopy analysis. Cells were transfected with the annexin A8-GFP expression plasmid, and the fusion protein was detected by immunolabeling the GFP moiety. As shown in Figure 2A, the annexin A8-GFP signal (10-nm protein A gold) was found at the limiting membrane of endosomes containing internal vesicular and lamellar structures, a pleiomorphic structural appearance typically found in the late endosomal compartment. These multivesicular endosomes also proved positive for LBPA (Figure 2B, 15-nm protein A gold), further indicating the late endosomal origin. In contrast to the clear labeling of the endosomal compartment seen by immuno-fluorescence, in the cryosections the majority of annexin A8-GFP is cytosolic. This difference is due to the methanol extraction of the cells used for immunofluorescence, which reduces the cytosolic pool (Figure 1). To address the annexin A8 distribution directly and to obtain a more quantitative analysis, we analyzed the Ca^{2+}-dependent cellular distribution of annexin A8-GFP by using subcellular fractionation. The membrane fraction and the cytosol were separated and analyzed for their respective amounts of the late endosomal/lysosomal marker LAMP2 and annexin A8-GFP (Figure 3A). As shown in Figure 3B, quantitative analysis of the annexin A8-GFP distribution revealed that ~13% of the ectopically expressed protein is found in the membrane pellet, whereas the majority (>80%) is found in the cytosolic fraction. Addition of Ca^{2+} during the cell lysis led to a significant translocation of annexin A8-GFP from the cytosol to the membrane fraction, a characteristic feature of annexins. To further discriminate between the different pools of the membrane bound annexin A8-GFP observed by fluorescence microscopy, we established single cell analysis of the annexin A8-GFP ratio associated with the plasma membrane

and endosomes, respectively. As shown in Figure 3C, plasma membrane bound annexin A8-GFP represented roughly 10% of all annexin A8-GFP signals found associated with membranes within a single cell, and >80% were found on endosomes.

Annexin A8 Controls the Morphological Appearance of the Multivesicular Late Endosomal Compartment

To investigate a possible role of annexin A8 in late endosome morphology and maintenance of the late endosomal compartment, we used RNA interference to reduce the expression of endogenous annexin A8. Transfection of HeLa cells with an annexin A8-specific siRNA duplex targeted to nucleotides 848–866 of the human annexin A8 cDNA sequence consistently resulted in an 80–90% reduction in the annexin A8 protein level after 48 h. Expression levels of other annexins, namely, those that have also been reported to play a role in endosomal dynamics, annexins A1 and A2, or the unrelated gene product vimentin, were not affected (Figure 4A; our unpublished data). Depending on the intracellular annexin A8 levels, we observed a marked difference in the localization and average size of LAMP1-positive endosomes. As shown in Figure 4B, LAMP1-positive endosomes in mock-transfected cells were slightly concentrated in the perinuclear region, whereas in annexin A8-depleted cells they were smaller and more scattered throughout the cell. In annexin A8-GFP–expressing cells, the LAMP1-positive endosomes seemed to be more condensed in the perinuclear region, with a significant increase in the average size of these endosomes and the appearance of a significant number of atypical "giant" vesicles (Figure 4, B and C). As shown in Figure 4D, quantitative analysis revealed that in annexin A8-GFP–expressing cells the average diameter of the LAMP1-positive endosomes (1.1 μm, on average, without the endosomes classified as "giant") increased by ~25%, whereas RNAi-mediated depletion of annexin A8 led to smaller endosomes with the average size (0.65 μm) being decreased to ~70% of LAMP1-positive endosomes in the respective control cells (0.9 μm). Expression of GFP alone neither affected the distribution nor the size of the late endosomes. The observed phenotype on the morphology of LAMP1-positive endosomes was also observed on down-regulation of annexin A8 with a second independent annexin A8-specific siRNA duplex (data not shown), arguing for the specificity of the phenotype.

To confirm that the smaller and more dispersed appearance of LAMP1-positive endosomes was a direct consequence of annexin A8 depletion, we performed rescue ex-
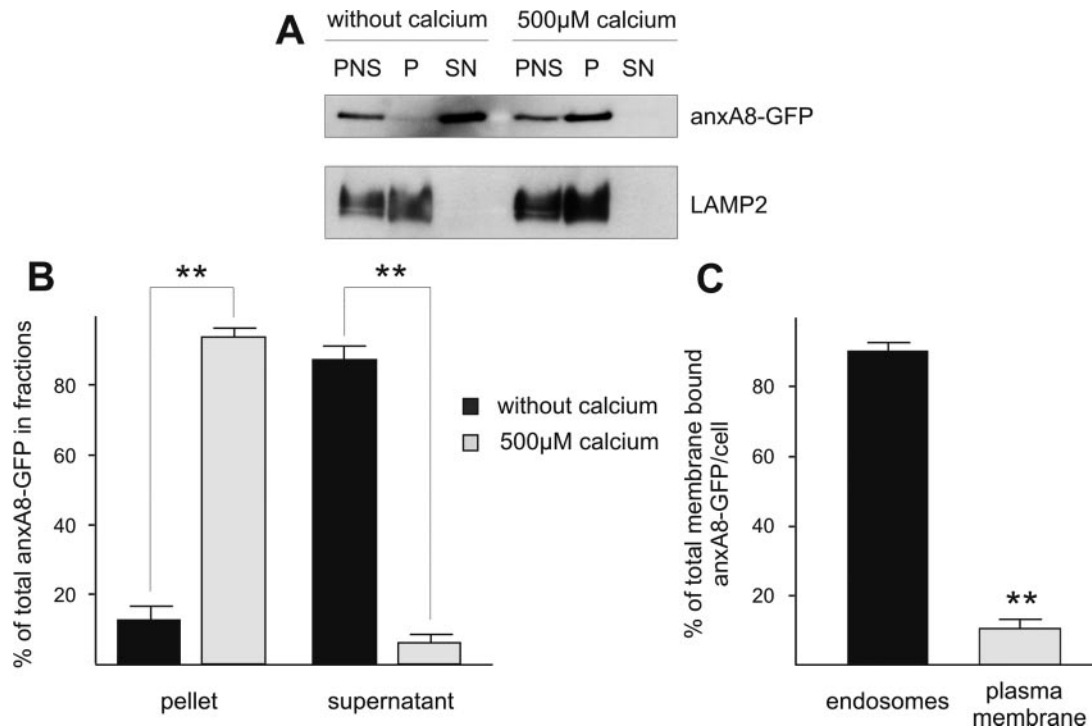
Figure 3. Membrane distribution of annexin A8. (A) Annexin A8 distributes Ca^{2+} dependently to the LAMP2-enriched membrane fraction. PNS of cells transfected with annexin A8-GFP were either prepared with or without addition of 500 μM Ca^{2+} and pelleted for 60 min at $100,000 \times g$ to obtain the membrane fraction. Equal protein amounts of PNS, membrane pellets, and supernatants were analyzed by SDS-PAGE and immunoblotting for LAMP2 and annexin A8-GFP. (B) Amounts of annexin A8-GFP in the pelleted membranes and the supernatants were calculated as percentage of total annexin A8-GFP by densitometric scanning of the immunoreactive bands. Bars represent the mean amount $\pm$ SEM of at least five independent experiments. **$p < 0.0005$. (C) To analyze the intracellular membrane association of annexin A8-GFP, quantitative single-cell analysis of digital fluorescence images was performed. The amount of annexin A8-GFP bound to the specific membranes was quantified by determining signal intensities from 20 cells, with the total membrane-bound annexin A8-GFP set as 100%. Bars represent the mean amount $\pm$ SEM **$p < 0.0005$.

periments analyzing the appearance of LAMP1-positive endosomes in annexin A8-depleted cells re-expressing annexin A8-GFP. Cells that had been treated with annexin A8 siRNA for 2 d were transfected with annexin A8-GFP and analyzed for both their amounts of endogenous annexin A8 and the ectopically expressed GFP-tagged version by Western blotting with the anti-annexin A8 antibody. As shown in Figure 5A, 24 h after annexin A8-GFP transfection the pool of endogenous annexin A8 was still depleted, but high amounts of annexin A8-GFP were detected. Morphological analysis revealed that annexin A8 re-expressing cells showed a distribution of the LAMP1-positive endosomes similar to that observed in nondepleted cells, whereas in cells that had escaped annexin A8-GFP transfection the abnormal dispersed distribution was still visible (Figure 5B). These results confirm that annexin A8 is a critical component for the maintenance of the correct distribution of the late endosomal/lysosomal compartment.

Immuno-electron microscopy (EM) analysis of the CD63/LAMP3-positive late endosomal compartment also reflected the size irregularity caused by altered cellular annexin A8 levels. To detect late endosomes, we immunolabeled the tetraspanin CD63/LAMP3, which is present on the limiting membrane as well as on the internal membranous structures of late endosomes. As shown in Figure 6A, the LAMP3-positive multivesicular late endosomes in annexin A8-GFP–expressing cells were considerably enlarged compared with those of GFP-transfected cells, with the diameters of these enlarged endosomes measured in random EM profiles cor-

responding to those established by light microscopy (see above). The control cells showed LAMP3-positive vesicles of normal size generally found in nontransfected HeLa cells (Figure 6B; our unpublished data). In annexin A8-depleted cells, the size of LAMP3-positive vesicles was markedly reduced (Figure 6C).

Annexin A8 Depletion Results in the Dispersal of Late Endosomes, the Delay of Late Endosomal Cargo Transport, and the Impairment of Ligand-induced Degradation of the EGF Receptor

We next examined whether the uptake and transport of cargo destined to enter the degradation pathway was altered in annexin A8 down-regulated cells. We therefore investigated the degradation of ligand-activated EGFR. On binding of the cognate ligand EGF, this receptor is rapidly endocytosed and sorted to internal vesicles of LBPA-positive multivesicular late endosomes to be ultimately degraded in late endosomes/lysosomes. We first evaluated the influence of annexin A8 levels on the internalization and degradation of EGF. Serum-starved cells were allowed to internalize rhodamine-conjugated EGF for different periods. As shown in Figure 7A, labeled EGF was detected in a scattered vesicular pattern upon an initial exposure for 10 min. No obvious difference in the localization of EGF could be observed at this time in the annexin A8-depleted cells. However, when control cells were further chased for 4 h, the signal accumulated in LAMP3-positive organelles clustered in the perinuclear region, whereas in annexin A8-depleted cells, labeled
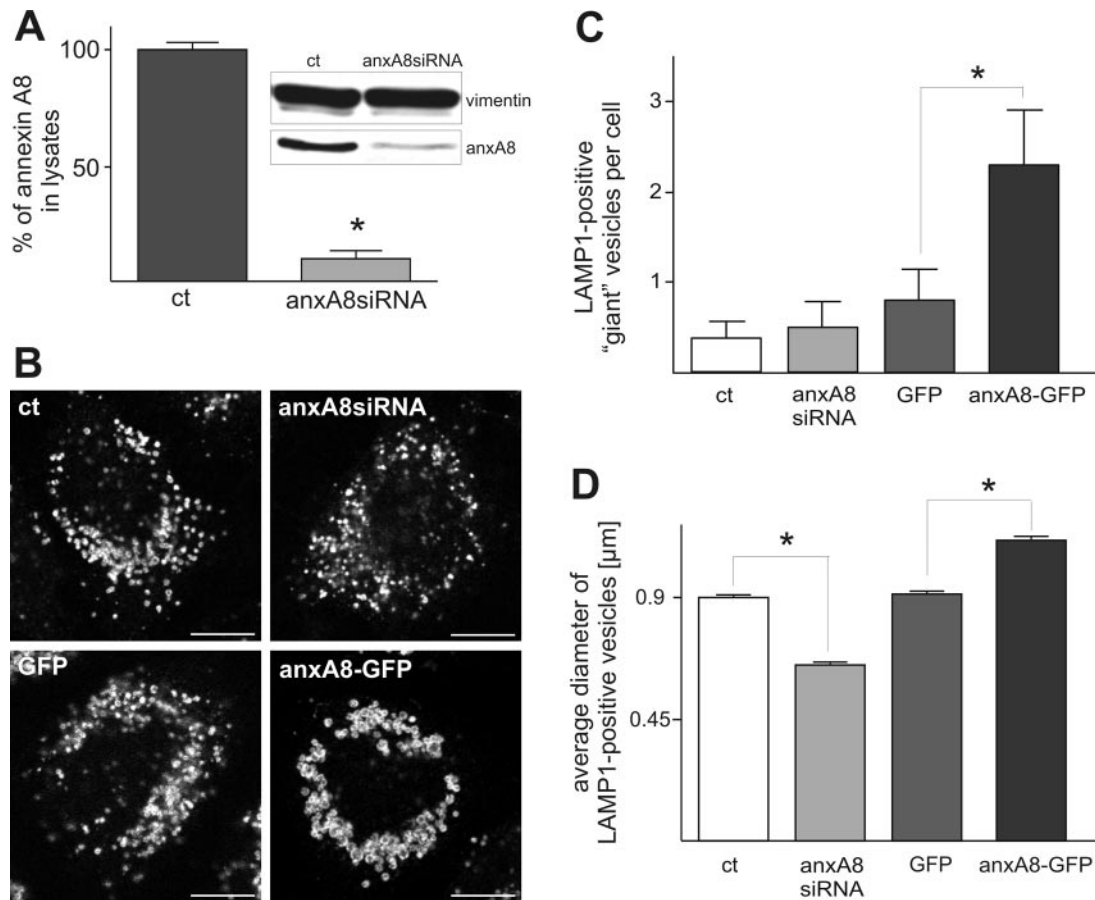
Figure 4. Annexin A8 controls the morphological appearance of the multivesicular late endosomal compartment. (A) Lysates of cells transfected for 48 h with either control siRNA (ct) or annexin A8-specific siRNA (anxA8siRNA) were analyzed by immunoblotting using anti-annexin A8 antibodies. Immunodetection of vimentin was used to ensure equal loadings. Amounts of endogenous annexin A8 in lysates were quantified by densitometric scanning. The bar graph presents the percentage of annexin A8 levels ± SEM from six different experiments, with the amount of annexin A8 in control cell lysate set as 100%, *p < 0.0001. (B) Cells transfected with control (ct) or annexin A8-specific siRNA (anxA8siRNA) or cells expressing GFP or annexin A8-GFP (anxA8-GFP) were stained with anti-LAMP1 antibodies. Images represent single confocal sections. Bars, 10 μm. (C) Relative number of LAMP1-positive "giant" endosomes per cell ± SEM, *p < 0.05. (D) To characterize the effects of annexin A8 levels in a quantitative manner, average diameters of LAMP1-positive endosomes ± SEM (excluding giant endosomes) from 10 individual cells each were determined. Control cells set as 100%, *p < 0.05.

EGF was found in smaller LAMP3-positive vesicles that seemed more scattered throughout the cell (Figure 7B). This indicates that annexin A8 does not control early stages of the endosomal pathway but functions in the regulation of transport to late endosomal compartments.

To determine the effect of this altered late endosomal positioning on the actual degradation of internalized EGF, we treated the cells with ^{125}I-EGF and followed the rate of degradation by measuring the amount of TCA-soluble [125]I. Delayed degradation of radiolabeled EGF in the annexin A8-depleted cells could be observed as early as 60 min after EGF incubation. Differences in the amount of degraded EGF became statistically significant 120 min after ^{125}I-EGF treatment (Figure 7C). Next, we analyzed the ligand-induced EGFR degradation to examine whether the observed differences in EGF degradation were due to altered EGFR degradation kinetics. HeLa cells transfected with either control or annexin A8-specific siRNA were serum starved overnight to accumulate EGFR at the plasma membrane. Cells were then stimulated with EGF for varying periods in the presence of cycloheximide to inhibit protein synthesis. Total cellular lysates were immunoblotted with anti-EGFR antibody (Figure 8A). Quantitative densitometric analysis revealed that a

significant loss in mature EGFR levels was detectable after 60 min of EGF stimulation in mock transfected cells, whereas in the annexin A8-depleted cells mature EGFR immunoreactivity was not decreased in this time interval (Figure 8B). After a chase period of 240 min, only minimal levels of intact mature EGFR could be detected in mock-transfected cells, whereas annexin A8 depleted cells still showed substantial amounts of nondegraded receptor.

Annexin A8 Depletion Results in Prolonged EGF-induced ERK1/2 Activation

Down-regulation of activated signaling receptors through endocytosis is an important means to regulate the strength and duration of signal transduction. Because EGFR degradation has a major impact on the regulation of EGF signaling, we next examined whether the observed delay in EGFR degradation is reflected in MAP kinase signaling. Because the half-life of EGF-bound activated EGFR was estimated to be ~60 min (Wiley, 2003), we focused on longer ligand exposure times. As shown in Figure 9, the delayed degradation of the EGFR observed in annexin A8 deficient cells resulted in a sustained ERK signaling. In mock-transfected
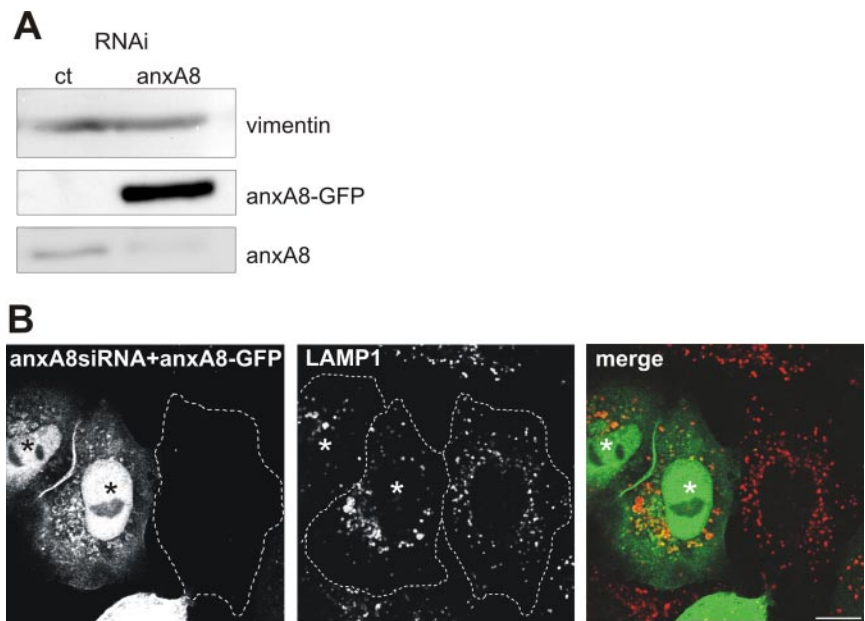
Figure 5. Re-expression of annexin A8-GFP in cells depleted of endogenous annexin A8 restores the perinuclear localization of LAMP1-positive endosomes. (A) Western blotting of total cell lysates shows that in cells depleted of endogenous annexin A8, annexin A8-GFP is expressed at a high level. (B) Annexin A8 siRNA-treated cells re-expressing annexin A8-GFP (asterisks) showed LAMP1-positive endosomes predominantly in the perinuclear region, whereas the nonrescued cell next to them still shows the dispersed distribution typically found in annexin A8-depleted cells. Bar, 10 μM.

HeLa cells, EGF-induced ERK phosphorylation is markedly declining within 120 min of EGF exposure. In contrast, substantial ERK activation could still be observed at that time point in annexin A8-depleted cells (Figure 9B).

### Annexin A8 Depletion Decreases the Association of Late Endosome-associated Endocytic Membranes with Actin

We have shown previously that annexin A8 interacts with F-actin in vitro and is recruited to membrane areas associated with dynamic actin rearrangement (Goebeler *et al.*, 2006). Altering annexin A8 levels did not change the overall appearance of the actin cytoskeleton (data not shown), arguing against a general role of the protein in the organization of the cellular actin network. Because annexin A8 specifically affects properties of late endosomes and because many observations link the actin cytoskeleton to late endosomal distribution, morphology, trafficking, and fusion (Jahraus *et al.*, 2001; Eitzen *et al.*, 2002; Kjeken *et al.*, 2004), we next analyzed whether annexin A8 regulates the association of actin with late endosomes.

As shown in Figure 10A, actin patches localized to many of the perinuclear annexin A8-GFP–positive endosomes in cells expressing annexin A8-GFP. To assess whether the actin cytoskeleton participates in mediating the effect of annexin A8 on the appearance of LAMP1-positive endosomes, we perturbed the actin filaments with the actin-interfering drugs latrunculin A and cytochalasin D, both potent inhibitors of actin polymer-

ization. Latrunculin A still permits lysosomes to move rapidly, but it impairs directed transport, leading to random movements (Cordonnier *et al.*, 2001). In cells that were treated with latrunculin A for 10 min, the annexin A8-positive vesicles seemed more disperse and were found closer to the plasma membrane (Figure 10B shows a representative image). This could be due to a decreased association of these endosomes with actin filaments, resulting in randomly directed movements. Cytochalasin D has been shown to decrease the ability of lysosomes to move by trapping them in actin patches throughout the cell (Cordonnier *et al.*, 2001). In line with the published observations, cells that were treated with cytochalasin D for 15 min showed a more dispersed distribution of LAMP1-positive endosomes (Figure 10C, top). In contrast, cells that were depleted of annexin A8 did not show further dispersion of LAMP1-positive endosomes upon cytochalasin D treatment (Figure 10C, middle and bottom).

Next, we determined the amount of actin-associated late endosomal membranes in annexin A8-depleted versus mock-transfected control cells, making use of cosedimentation assays described previously (Holtta-Vuori *et al.*, 2005). LAMP2-positive membrane fractions were pelleted from the postnuclear supernatants of cell lysates and analyzed for the amount of LAMP2, which is highly enriched in late endosomes/lysosomes (Escola *et al.*, 1998), and actin. To exclude the pelleting of microtubule-associated membranes, lysates were treated with

Figure 6. Overexpression and suppression of annexin A8-GFP affect the size of late endosomes. Late endosomal compartments were labeled with CD63/LAMP3 antibodies followed by 15-nm protein A gold. Anti-GFP antibodies and 10-nm protein A gold was used to detect GFP. (A) CD63/LAMP3-positive late endosomes found in annexin A8-GFP–expressing cells are considerably enlarged. (B) A normal-sized lysosome of HeLa cells transfected with a GFP vector without insert. (C) Smaller CD63/LAMP3-positive late endosomes are found in annexin A8-depleted cells. Bars, 200 nm.
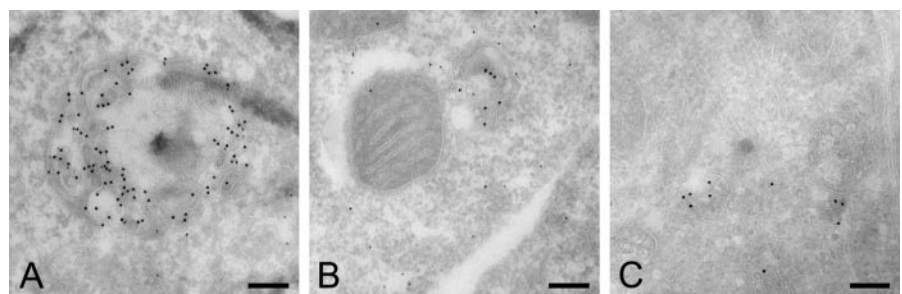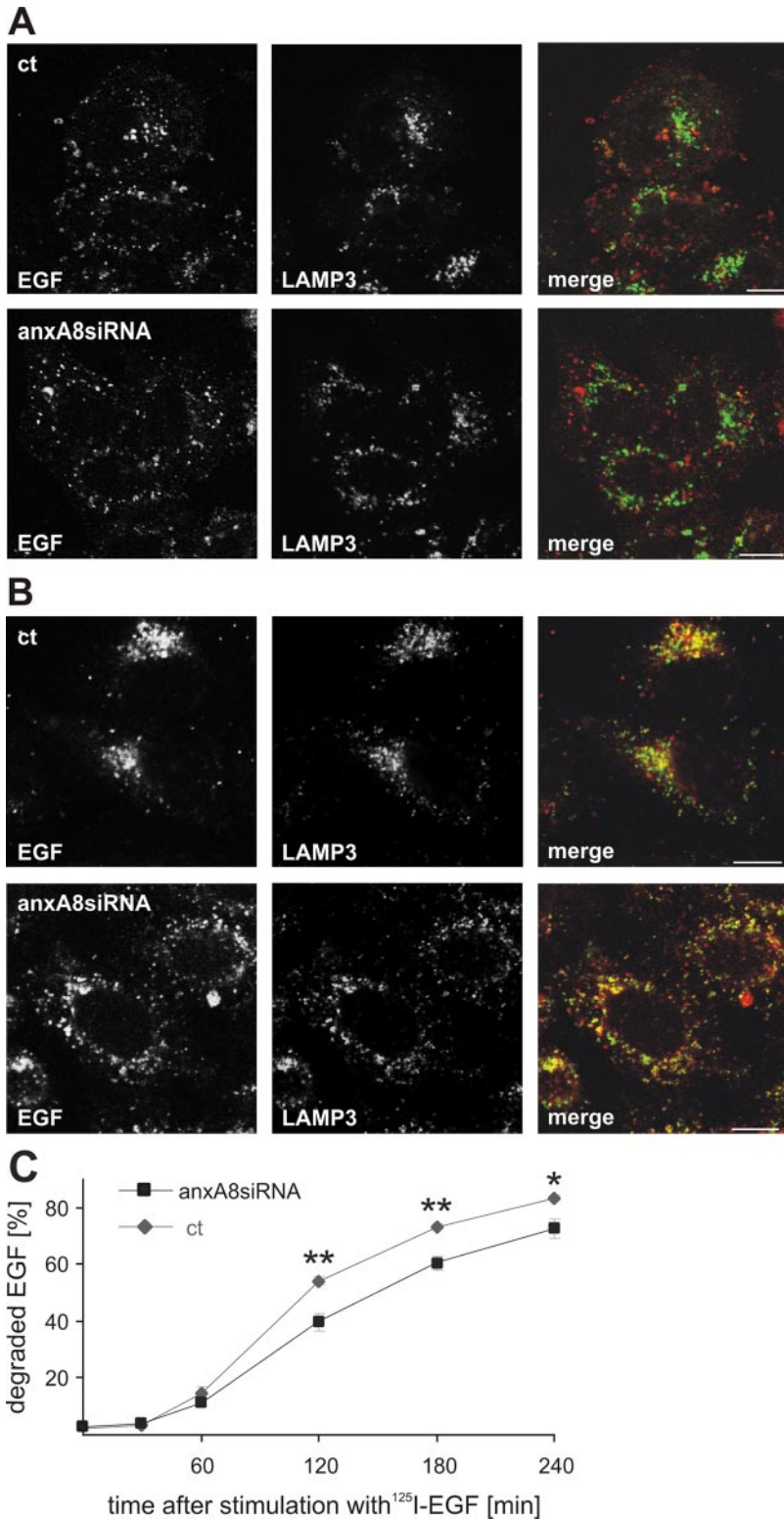
Figure 7. Annexin A8 depletion impairs EGF transport and degradation. Annexin A8-depleted (anxA8siRNA) cells were serum-starved overnight. (A) Rhodamine-coupled EGF was internalized for 10 min. (B) EGF uptake was followed by a 4-h chase period. Fixed cells were stained for LAMP3. Images represent single confocal sections. Bars, 10 μm. (C) Cells were incubated for 10 min with radiolabeled EGF and then chased for the indicated periods. EGF degradation was detected by measuring the release of TCA-soluble degradation products in the medium. Data are mean values $\pm$ SEM from four independent experiments. *p $<$ 0.05, **p $<$ 0.005.

nocodazole. As reported previously (Holtta-Vuori *et al.*, 2005), addition of cytochalasin D that served as an internal control of the assay caused a significantly reduced recovery of LAMP2 in the pellet (data not shown). Significantly less actin-associated LAMP2 was also recovered from annexin A8-depleted cells compared with mock-transfected cells (Figure 11, A and B), indicating that annexin A8 as an F-actin and membrane-bind-ing protein might function in regulating the association of late endosomes with actin filaments.

DISCUSSION

Endosomal organelles move actively along cytoskeletal elements to maintain their respective spatial organization in the
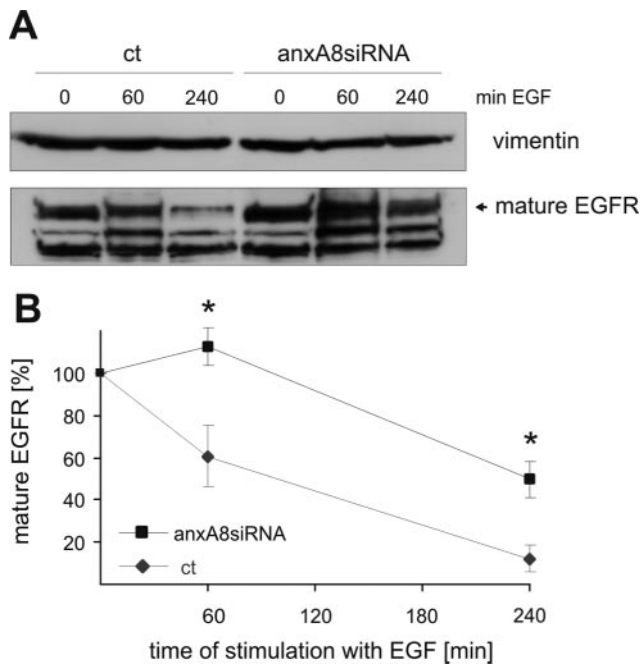
Figure 8. Depletion of annexin A8 impairs ligand-induced EGFR degradation. HeLa cells transfected for 48 h with control siRNA (ct) or annexin A8-specific siRNA (anxA8siRNA) were serum starved overnight and then treated with 100 ng/ml EGF in the presence of cycloheximide for the indicated periods. Degradation of EGFR was analyzed by immunoblotting cell lysates with anti-EGFR antibodies. In A, a representative immunoblot from five independent experiments is shown. Vimentin was used as a control to ensure equal loading of total cellular proteins. (B) Kinetics of EGFR degradation was assessed by densitometric quantification of the 180-kDa band corresponding to mature EGFR, and expressed as the percentage of the EGFR level of cells at 0 min. Data represent mean values ± SEM from five independent experiments. *p < 0.02.
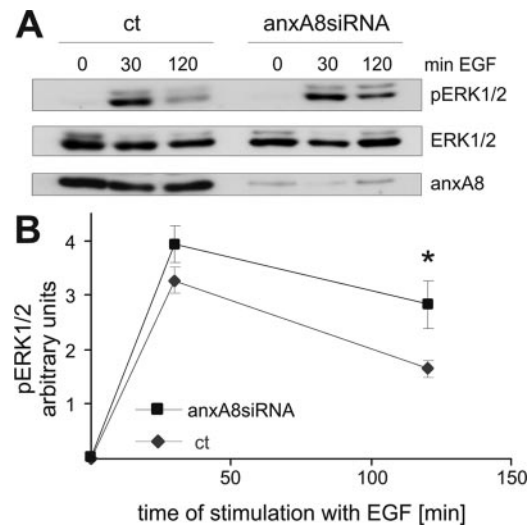

Figure 9. Annexin A8 depletion results in sustained EGF-mediated ERK1/2 activation. HeLa cells transfected for 48 h with control siRNA (ct) or annexin A8-specific siRNA (anxA8siRNA) were serum starved overnight and then treated with 100 ng/ml EGF for the indicated times. The activation state of the MAP kinases ERK1/2 was assessed by immunoblotting the cell lysates with phospho-specific ERK1/2 antibodies. Total levels of ERK and annexin A8 in the lysates were detected with anti-ERK and anti-annexin A8 antibodies, respectively. In A, a typical blot is shown. (B) The time course of EGF-induced MAP kinase activation is presented after normalizing for total ERK loading. Data represent mean values ± SEM from five independent experiments. *p < 0.05.

cell. The proper localization of the endocytic compartments is thought to be critically important for their proper physiological functions. Microtubules mediate long-range transport of organelles of the degradative pathway, whereas actin filaments are thought to be also required for the proper distribution, probably supporting efficient fusion (for reviews, see Gruenberg and Stenmark, 2004; Piper and Katzmann, 2007). These processes are particularly relevant in the endocytic down-regulation of ligand-activated receptors to decrease the levels of signaling receptors and thereby ensure proper termination of signal transduction. Inappropriate persistence of stimulation of such receptors is implicated in the development of diseases such as cancer and autoimmune disorders. Here, we identified the F-actin and phospholipid binding protein annexin A8 as specifically associated with endosomal vesicles that contain specific markers for multivesicular late endosomes (Gruenberg and Stenmark, 2004). In addition, electron microscopy of the annexin A8-positive organelles revealed the pleiomorphic structure of multivesicular, tubular, and cisternal regions seen in late endosomes, comprising internal vesicles and membrane sheets of different densities. Altering intracellular annexin A8 levels altered the localization of the LAMP-positive vesicles as well as late endosomal diameter, suggesting that annexin A8 contributes to the correct positioning and morphological appearance of the late endosomal compartment.

Annexin A8 belongs to the annexin protein family of Ca^{2+}-binding proteins. Their highly conserved so-called "core" mod-

ule bears the unique Ca^{2+}-binding sites that mediate a Ca^{2+}-dependent, reversible binding to cellular membranes (Gerke et al., 2005). Some annexins also interact with F-actin filaments and certain phosphatidylinositides such as phosphatidylinositol (4,5)-bisphosphate [PtdIns(4,5)P$_2$] (Hayes et al., 2004; Rescher and Gerke, 2004). Due to their properties, they might form membrane scaffolds that organize and/or stabilize certain membrane domains and in some cases link them to the underlying actin cytoskeleton (for review, see Hayes et al., 2004). Recent studies demonstrated that annexin A2 and annexin A1 function in the endocytic pathway (Mayran et al., 2003; Zobiack et al., 2003; White et al., 2006), although their precise mechanism of action is not known. Our finding that annexin A8 is involved in the late endosomal-associated actin dynamics provides a mechanistic explanation of the observed annexin A8 effects.

Interestingly, altering annexin A8 levels did not cause obvious changes in early endocytic events such as EGF uptake. However, trafficking along the degradative pathway was slowed down in annexin A8-depleted cells and this correlated with defective degradation of both the EGFR and its cognate ligand. The observation that EGFR degradation was delayed in annexin A8-depleted cells for ~60 min but then seemed to proceed at a rate comparable with control cells suggests that a transport step rather than receptor degradation per se was affected.

The EGF/EGFR system is a well-studied model system for the coupling of ligand-induced endocytic down-regulation to the signaling potential. In contrast to other members of the ErbB family, EGFR signaling occurs from within the endosomes. Thus, trafficking of the receptor-ligand complex through the different compartments not only regulates the levels of activated signaling receptor but also ensures proper temporal and spatial control of EGF-mediated signaling to
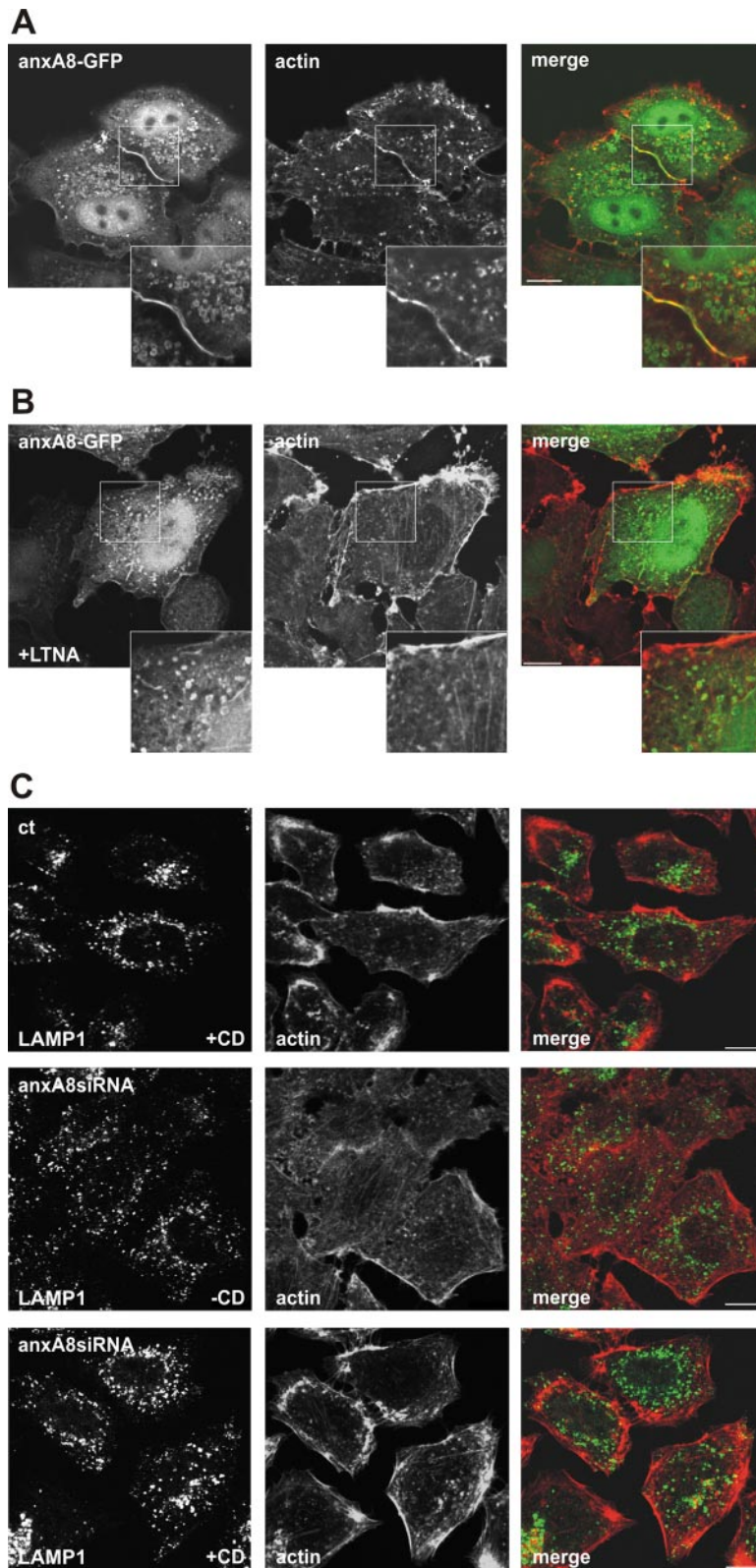
Figure 10. Perturbation of the actin cytoskeleton affects the annexin A8-mediated alterations in late endosomal appearance. (A) Actin patches visualized with anti-actin antibody are often found in proximity to clustered annexin A8-GFP–positive endosomes in annexin A8-GFP–expressing cells. In B, cells were treated with LTNA to interfere with actin polymerization. Note the more dispersed distribution of annexin A8-GFP–positive endosomes compared with untreated cells. Compared with the actin stain shown in A, the image shown in B was recorded with a longer exposure time to visualize the remaining actin-positive structures. (C) Distribution of LAMP1-positive endosomes in cells treated with CD. In contrast to control cells that display dispersed LAMP1-positive endosomes upon CD treatment (ct; top) CD does not affect the localization of LAMP1-positive endosomes in annexin A8-depleted cells (anxA8siRNA, middle and bottom). Bars, 10 μm. Insets show a twofold magnification of the boxed regions.

various downstream effectors (Jorissen *et al.*, 2003; Wiley, 2003). Accordingly, changes in the EGFR degradation kinetics, as has been achieved through manipulating mediators of vesicular trafficking, such as dynein and Rab7 (Taub *et al.*, 2007), or by expression of EGFR mutants, were shown to

result in prolonged and sustained MAP kinase signaling. Consistently, we observed that the delayed transport and degradation of activated EGFR in annexin A8-depleted cells correlated with prolonged EGF-induced ERK activation. Interestingly, annexin A8 overexpression did not cause detect-
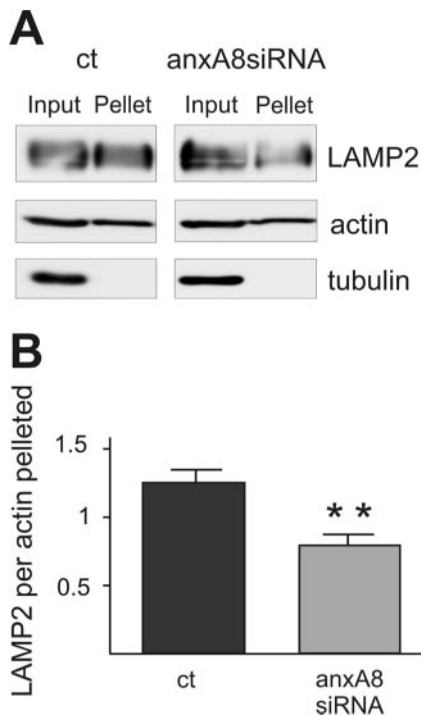
Figure 11. Annexin A8 depletion reduces the association of LAMP2-positive membranes with F-actin. Membranes from post-nuclear supernatants (input) of cells transfected with control (ct) or annexin A8-specific siRNA (anxA8siRNA) were pelleted by centrifugation and analyzed for their actin and LAMP2 contents. To exclude the pelleting of microtubule-associated membranes, lysates were treated with nocodazole and the recovered membrane fractions were probed for tubulin. (A) A representative blot. (B) To normalize the different experiments, LAMP2 and actin signals in the pelleted membranes were calculated as percentage of input by densitometric scanning of the respective immunoreactive bands. Bars represent the mean amount $\pm$ SEM of actin-associated LAMP2 in the pellets of 11 independent experiments. *$p < 0.03$.

able changes in the kinetics of EGF degradation and EGFR down-regulation, although the morphology of the late endosomes was severely altered in these cells. It is likely that the increase in diameter observed in annexin A8 overexpressing cells is caused by homotypic fusion of late endosomes. This could occur following annexin A8-mediated clustering of these organelles resulting in increased proximity and fusion probability without affecting EGFR degradation within the fused organelles.

The characteristic perinuclear steady-state localization of late endosomes and lysosomes is thought to depend both on microtubules as well as actin filaments (Matteoni and Kreis, 1987; Cordonnier *et al.*, 2001; Taunton, 2001). Whereas several components of the microtubule-dependent movement of late endosomes have been identified, such as the GTPase Rab7, the effector RILP that attaches late endosomes to the dynein/dynactin complex of motor proteins (Jordens *et al.*, 2001; Progida *et al.*, 2007), or kinesins (Hoepfner *et al.*, 2005), actin-dependent late endosomal transport is less well understood. Pharmacological disruption of the actin cytoskeleton impairs receptor degradation in several cellular models (van Deurs *et al.*, 1995; Durrbach *et al.*, 1996) and relocalizes late endosomes to the cell periphery. Perinuclear aggregation and both fusion of late endosomes with each other or with lysosomes, critically depend on actin (van Deurs *et al.*, 1995; Jahraus *et al.*, 2001; Kjeken *et al.*, 2004). Likewise, homotypic

vacuole fusion in yeast that is analogous to mammalian late endosomal/lysosomal fusion requires actin (Eitzen *et al.*, 2002). Further emphasizing a link to the actin cytoskeleton, late endosomes/lysosomes can nucleate F-actin on their membranes (Taunton *et al.*, 2000; Jahraus *et al.*, 2001; Kjeken *et al.*, 2004), thereby presumably assembling actin filaments to facilitate fusion with neighboring organelles. Based on our results, we propose that annexin A8 present on the limiting membrane of late endosomes might link late endosomes to the actin cytoskeleton through either direct interaction or through the organization of specific membrane/actin attachment sites. Disruption of this action, for example by annexin A8 depletion, interferes with the proper localization of late endosomes and, as a consequence, impairs cargo transport through the endocytic pathway resulting in imbalanced signaling patterns.

REFERENCES

Cordonnier, M. N., Dauzonne, D., Louvard, D., and Coudrier, E. (2001). Actin filaments and myosin I alpha cooperate with microtubules for the movement of lysosomes. Mol. Biol. Cell *12*, 4013–4029.

Durrbach, A., Louvard, D., and Coudrier, E. (1996). Actin filaments facilitate two steps of endocytosis. J. Cell Sci. *109*, 457–465.

Eitzen, G., Wang, L., Thorngren, N., and Wickner, W. (2002). Remodeling of organelle-bound actin is required for yeast vacuole fusion. J. Cell Biol. *158*, 669–679.

Escola, J. M., Kleijmeer, M. J., Stoorvogel, W., Griffith, J. M., Yoshie, O., and Geuze, H. J. (1998). Selective enrichment of tetraspan proteins on the internal vesicles of multivesicular endosomes and on exosomes secreted by human B-lymphocytes. J. Biol. Chem. *273*, 20121–20127.

Gerke, V., Creutz, C. E., and Moss, S. E. (2005). Annexins: linking Ca^{2+} signalling to membrane dynamics. Nat. Rev. Mol. Cell Biol. *6*, 449–461.

Goebeler, V., Ruhe, D., Gerke, V., and Rescher, U. (2006). Annexin A8 displays unique phospholipid and F-actin binding properties. FEBS Lett. *580*, 2430–2434.

Griffiths, G., Hoflack, B., Simons, K., Mellman, I., and Kornfeld, S. (1988). The mannose 6-phosphate receptor and the biogenesis of lysosomes. Cell *52*, 329–341.

Gruenberg, J., and Stenmark, H. (2004). The biogenesis of multivesicular endosomes. Nat. Rev. Mol. Cell Biol. *5*, 317–323.

Hayes, M. J., Rescher, U., Gerke, V., and Moss, S. E. (2004). Annexin-actin interactions. Traffic *5*, 571–576.

Hoepfner, S., Severin, F., Cabezas, A., Habermann, B., Runge, A., Gillooly, D., Stenmark, H., and Zerial, M. (2005). Modulation of receptor recycling and degradation by the endosomal kinesin KIF16B. Cell *121*, 437–450.

Holtta-Vuori, M., Alpy, F., Tanhuanpaa, K., Jokitalo, E., Mutka, A. L., and Ikonen, E. (2005). MLN64 is involved in actin-mediated dynamics of late endocytic organelles. Mol. Biol. Cell *16*, 3873–3886.

Jahraus, A., Egeberg, M., Hinner, B., Habermann, A., Sackman, E., Pralle, A., Faulstich, H., Rybin, V., Defacque, H., and Griffiths, G. (2001). ATP-dependent membrane assembly of F-actin facilitates membrane fusion. Mol. Biol. Cell *12*, 155–170.

Jordens, I., Fernandez-Borja, M., Marsman, M., Dusseljee, S., Janssen, L., Calafat, J., Janssen, H., Wubbolts, R., and Neefjes, J. (2001). The Rab7 effector protein RILP controls lysosomal transport by inducing the recruitment of dynein-dynactin motors. Curr. Biol. *11*, 1680–1685.

Jorissen, R. N., Walker, F., Pouliot, N., Garrett, T. P., Ward, C. W., and Burgess, A. W. (2003). Epidermal growth factor receptor: mechanisms of activation and signalling. Exp. Cell Res. *284*, 31–53.

Katzmann, D. J., Odorizzi, G., and Emr, S. D. (2002). Receptor downregulation and multivesicular-body sorting. Nat. Rev. Mol. Cell Biol. *3*, 893–905.

Kjeken, R. *et al.* (2004). Fusion between phagosomes, early and late endosomes: a role for actin in fusion between late, but not early endocytic organelles. Mol. Biol. Cell *15*, 345–358.

Kobayashi, T., Stang, E., Fang, K. S., de Moerloose, P., Parton, R. G., and Gruenberg, J. (1998). A lipid associated with the antiphospholipid syndrome regulates endosome structure and function. Nature *392*, 193–197.

Lange, C., Starrett, D. J., Goetsch, J., Gerke, V., and Rescher, U. (2007). Transcriptional profiling of human monocytes reveals complex changes in the expression pattern of inflammation-related genes in response to the annexin A1-derived peptide Ac1-25. J. Leukoc. Biol. *82*, 1592–1604.

Liou, W., Geuze, H. J., and Slot, J. W. (1996). Improving structural integrity of cryosections for immunogold labeling. Histochem. Cell Biol. *106*, 41–58.

Matsuo, H. *et al.* (2004). Role of LBPA and Alix in multivesicular liposome formation and endosome organization. Science *303*, 531–534.

Matteoni, R., and Kreis, T. E. (1987). Translocation and clustering of endosomes and lysosomes depends on microtubules. J. Cell Biol. *105*, 1253–1265.

Mayran, N., Parton, R. G., and Gruenberg, J. (2003). Annexin II regulates multivesicular endosome biogenesis in the degradation pathway of animal cells. EMBO J. *22*, 3242–3253.

Piper, R. C., and Katzmann, D. J. (2007). Biogenesis and function of multivesicular bodies. Annu. Rev. Cell Dev. Biol. *23*, 519–547.

Piper, R. C., and Luzio, J. P. (2007). Ubiquitin-dependent sorting of integral membrane proteins for degradation in lysosomes. Curr. Opin. Cell Biol. *19*, 459–465.

Progida, C., Malerod, L., Stuffers, S., Brech, A., Bucci, C., and Stenmark, H. (2007). RILP is required for the proper morphology and function of late endosomes. J. Cell Sci. *120*, 3729–3737.

Rescher, U., and Gerke, V. (2004). Annexins–unique membrane binding proteins with diverse functions. J. Cell Sci. *117*, 2631–2639.

Richardson, S. C., Winistorfer, S. C., Poupon, V., Luzio, J. P., and Piper, R. (2004). Mammalian late vacuole protein sorting orthologues participate in early endosomal fusion and interact with the cytoskeleton. Mol. Biol. Cell *15*, 1197–1210.

Slot, J. W., Geuze, H. J., Gigengack, S., Lienhard, G. E., and James, D. E. (1991). Immuno-localization of the insulin regulatable glucose transporter in brown adipose tissue of the rat. J. Cell Biol. *113*, 123–135.

Taub, N., Teis, D., Ebner, H. L., Hess, M. W., and Huber, L. A. (2007). Late endosomal traffic of the epidermal growth factor receptor ensures spatial and temporal fidelity of mitogen-activated protein kinase signaling. Mol. Biol. Cell *18*, 4698–4710.

Taunton, J. (2001). Actin filament nucleation by endosomes, lysosomes and secretory vesicles. Curr. Opin. Cell Biol. *13*, 85–91.

Taunton, J., Rowning, B. A., Coughlin, M. L., Wu, M., Moon, R. T., Mitchison, T. J., and Larabell, C. A. (2000). Actin-dependent propulsion of endosomes and lysosomes by recruitment of N-WASP. J. Cell Biol. *148*, 519–530.

van der Goot, F. G., and Gruenberg, J. (2006). Intra-endosomal membrane traffic. Trends Cell Biol. *16*, 514–521.

van Deurs, B., Holm, P. K., Kayser, L., and Sandvig, K. (1995). Delivery to lysosomes in the human carcinoma cell line HEp-2 involves an actin filament-facilitated fusion between mature endosomes and preexisting lysosomes. Eur. J. Cell Biol. *66*, 309–323.

White, I. J., Bailey, L. M., Aghakhani, M. R., Moss, S. E., and Futter, C. E. (2006). EGF stimulates annexin 1-dependent inward vesiculation in a multivesicular endosome subpopulation. EMBO J. *25*, 1–12.

Wiley, H. S. (2003). Trafficking of the ErbB receptors and its influence on signaling. Exp. Cell Res. *284*, 78–88.

Zobiack, N., Rescher, U., Ludwig, C., Zeuschner, D., and Gerke, V. (2003). The annexin 2/S100A10 complex controls the distribution of transferrin receptor-containing recycling endosomes. Mol. Biol. Cell *14*, 4896–4908.